LES–Lagrangian-particles-simulation of turbulent reactive flows at high Sc number using approximate deconvolution model

T. Watanabe[1, a)] and K. Nagata[1]

Department of Aerospace Engineering, Nagoya University, Nagoya, 464-8603, Japan

Large eddy simulation (LES) with the approximate deconvolution model (ADM) is combined with Lagrangian particles simulation (LPS) for simulating turbulent reactive flows at high Schmidt numbers Sc. The LES is used to simulate velocity and nonreactive scalar while reactive scalars are simulated by the LPS using the mixing volume model for molecular diffusion. The LES–LPS is applied to turbulent scalar mixing layers with a second-order isothermal irreversible reaction at $Sc = 600$. The mixing volume model is implemented with the IEM, Curl's, and modified Curl's mixing schemes. The mixing volume model provides a correct decay rate of nonreactive scalar variance at high Sc independently of the number of particles. The statistics in the LES–LPS with the IEM or modified Curl's mixing scheme agree well with the experiments for both moderately-fast and rapid reactions. However, the LPS with the Curl's mixing scheme overpredicts the effects of the rapid reaction.

Keywords: Transport Phenomena and Fluid Mechanics, Large eddy simulation, Computational fluid dynamics (CFD), Mixing, Turbulence, Diffusion (mass transfer, heat transfer)

[a)] watanabe.tomoaki@c.nagoya-u.jp

INTRODUCTION

Turbulent mixing with chemical reactions can be observed in various pieces of industrial equipment and in the environment. Large eddy simulation (LES) has been one of the most common tools to predict turbulent flows, and it is expected to be applicable to chemical reactions in engineering and environmental flows. Applications of LES to reactive flows have been studied especially for turbulent combustions.[1] Chemical reactions in turbulent flows are strongly affected by the mixing process. The Schmidt number $Sc = \nu/D$ is an important parameter which characterizes mixing in turbulent flows (ν: kinematic viscosity, D: diffusivity coefficient of diffusive species). The mixing in gaseous flows, such as turbulent combustion problems, is characterized by a Schmidt number close to unity ($Sc \sim 1$). Much higher Sc can be seen in liquid flows, where the Schmidt number is of the order of 10^2–10^3. Reactive flows at high Sc are also practically important because they can be observed in chemical reactors and pollutant formations in ocean and rivers.

In LES, a filtering procedure is used for dividing velocity and scalar fields into large-scale and small-scale parts. LES resolves large-scale fields whereas the effects of unresolved small-scale, called subgrid scale (SGS), have to be modeled. The Batchelor scale $\eta_{\mathrm{B}} = \eta_{\mathrm{K}}/Sc^{1/2}$, which is the smallest scale of the scalar fluctuation, changes depending on the Schmidt number. Because of the difference in the length scales characterizing the scalar fields, it is not clear whether the numerical methods developed for reactive flows at low Sc can be applied to the flows at higher Sc. For example, Michioka et al.[2] showed that a model parameter used for modeling the SGS scalar variance depends on Sc. In LES of turbulent reactive flows, the filtered reaction source terms appear in an unclosed form in the filtered scalar transport equations.[3] Although the models for the filtered reaction source terms have been studied,[2,4] the characteristics of reactions can affect the performance of these models. Therefore, LES is often combined with the probability density function (PDF) method,[5] which does not require modeling of the reaction source terms. The LES–PDF approach has been developed based on the LES using the eddy viscosity model for the SGS Reynolds stress and the gradient diffusion model for the SGS scalar flux.[6] The eddy viscosity is used in various models, e.g., the Smagorinsky model and the dynamic Smagorinsky model. Bogey and Bailly reported that the eddy viscosity model can reduce the effective Reynolds number.[7] It is also known that the Smagorinsky model is too dissipative.[8] The dynamic

Smagorinsky model uses the model parameter which is dynamically computed. In this model, the spatial average is often used for computing the model parameter to prevent numerical instability[9] although spatial averaging might be inadequate for the flows consisting of turbulent, nonturbulent, and transition regions, because the SGS eddy viscosity changes between turbulent and nonturbulent regions.[10]

Stolz and Adams proposed the approximate deconvolution model[11] (ADM), which shows better performances than the Smagorinsky model or the dynamic Smagorinsky model.[8] The ADM computes the SGS terms using the small-scale fields approximately reconstructed from the large-scale fields. In LES based on the ADM, flows are divided into the filtered scale, subfilter scale, and subgrid (unresolved) scale.[12] The spatial low-pass filter in the LES has no direct influences on the filtered scale. The subgrid scale cannot be represented on the computational grid because of the lack of the spatial resolution. The subfilter scale is suppressed or removed by the filter, but the computational grid is small enough to resolve the subfilter scale. The filtered and subfilter scales are referred to as the resolved scale. The ADM can reconstruct the subfilter scale while the dissipations in the SGS are emulated by the relaxation terms or the low-pass filtering. The ADM can be applied to transitional flows consisting of laminar and turbulent flows without adjusting the model.[8,13] The LES with the ADM has been applied to various flows, such as decaying compressible isotropic turbulence,[11] channel flows,[8,13] round jets in a cross flow,[14] and turbulent supersonic boundary layers,[15] and succeeded to reproduce turbulence characteristics observed in other direct numerical simulations (DNS) or experiments.

These successes of the ADM motivate the application of the LES with the ADM to turbulent reactive flows. However, the reactions are sensitive to the subgrid scale, which cannot be reconstructed by the ADM. Therefore, the authors developed the combined approach between the LES with the ADM and the Lagrangian particles simulation (LPS).[16] In the LES–LPS, the velocity and nonreactive scalar are simulated by the LES with the ADM. The reactive scalars are simulated using a large number of Lagrangian notional particles because the reaction source terms appear in a closed form for the Lagrangian expressions of reactive scalar transport equations. In the LPS, the molecular diffusion terms have to be modeled. We proposed the mixing volume model based on the interaction among spatially-distributed multiple particles for modeling the molecular diffusion effects in the LES–LPS. The mixing model is also used for the molecular diffusion effects in the PDF methods. The conven-

tional mixing models used in the PDF methods also use the interaction among Lagrangian particles. In the conventional mixing models, the separation between the mixing particles is treated as the source of error due to the numerical diffusion.[17] In contrast, the mixing volume model yields a correct scalar dissipation rate even if the mixing particles are spatially distributed.[16] The LES–LPS based on the ADM and mixing volume model was tested for turbulent planar jets with a second-order isothermal irreversible reaction at $Sc = 1$.[16] The reactive scalar statistics showed good agreements between the LES–LPS and the reference DNS.

The purpose of this study is to apply the LES–LPS based on the ADM and mixing volume model to turbulent reactive flows at higher Sc. Using the LES–LPS, we simulate turbulent scalar mixing layers behind a turbulence-generating grid with a second-order isothermal irreversible reaction, which were investigated in liquid in the experiments by Komori et al.[18,19] The Schmidt number in their experiments is about 600. By comparing the concentration statistics of chemical species between the experiments and the LES–LPS, we will show that the LES–LPS is a useful tool to predict mixing and reactions at high Sc.

LES–LPS BASED ON THE ADM AND MIXING VOLUME MODEL

Large eddy simulation based on the ADM

An incompressible fluid with a nonreactive passive scalar transfer is considered in the present paper. The governing equations for velocity U_i and nonreactive passive scalar ψ are the continuity equation, the momentum equations, and the scalar transport equation. The following filtered equations are used in the LES,

$$\frac{\partial \overline{U_j}}{\partial x_j} = 0, \tag{1}$$

$$\frac{\partial \overline{U_i}}{\partial t} + \frac{\partial \overline{U_j U_i}}{\partial x_j} = -\frac{\partial \overline{P}}{\partial x_i} + \nu \frac{\partial^2 \overline{U_i}}{\partial x_j \partial x_j}, \tag{2}$$

$$\frac{\partial \overline{\psi}}{\partial t} + \frac{\partial \overline{U_j \psi}}{\partial x_j} = D \frac{\partial^2 \overline{\psi}}{\partial x_j \partial x_j}, \tag{3}$$

where P is the instantaneous pressure divided by the constant density ρ, ν is the kinematic viscosity, and D is the diffusivity coefficient for ψ. The spatial filtering operator G is defined

by

$$\overline{f}(x,y,z) \equiv G * f \equiv \int_{-\infty}^{\infty}\int_{-\infty}^{\infty}\int_{-\infty}^{\infty} G(x-x',y-y',z-z')f(x',y',z')dx'dy'dz'. \quad (4)$$

In the LES, the SGS models are required for the nonlinear term $\partial\overline{U_jU_i}/\partial x_j$ and the convective transport term $\partial\overline{U_j\psi}/\partial x_j$.

The ADM approximately reconstructs the unfiltered quantities using the approximate deconvolution filter $Q_N \approx G^{-1}$, where G^{-1} is the inverse filter defined by $f \equiv G^{-1} * \overline{f}$. The van Cittert deconvolution method[11] is used in the ADM to obtain Q_N as $Q_N = \sum_{n=0}^{N_\mathrm{D}}(I-G)^n$, where I is the identity operator. N_D is treated as a model parameter in the ADM. The ADM is often used with $N_\mathrm{D} = 5$ because of the insensitivity of the LES results to N_D for $N_\mathrm{D} \geq 5$.[8,13,16] The unfiltered value $\tilde{f}$ is approximately computed by $\tilde{f} = Q_N * \overline{f}$. In the ADM, $\tilde{U}_i$ and $\tilde{\psi}$ are used to compute the nonlinear term and the convective transport term. It should be noted that $\tilde{f}$ contains only the filtered and subfilter scales. The effects of the unresolved scale are modeled by the secondary filter $(Q_N * G)$, which is applied to the velocity and scalar fields.[13] This secondary filter removes the energy from the scales close to the smallest scale represented by the computational grid, and models the dissipations in the unresolved scale.[20] In the LES based on the relaxation filtering, the energy dissipation is accounted for by the numerical filtering.[21]

Lagrangian particles simulation (LPS)

The LPS of reactive scalars is combined with the LES. We consider N_S passive scalars $\mathbf{\Phi}(\mathbf{x},t) = (\phi_1(\mathbf{x},t),\ldots,\phi_\alpha(\mathbf{x},t),\ldots,\phi_{N_\mathrm{S}}(\mathbf{x},t))$, whose evolution is given by

$$\frac{\partial\phi_\alpha}{\partial t} + \frac{\partial U_j\phi_\alpha}{\partial x_j} = D_\alpha\frac{\partial^2\phi_\alpha}{\partial x_j\partial x_j} + S_\alpha(\mathbf{\Phi}), \quad (5)$$

where D_α is the diffusivity coefficient for ϕ_α and S_α is the reaction source term for ϕ_α, which is a function of $\mathbf{\Phi}$. We introduce the Lagrangian notional particles whose state is represented by the position $\mathbf{x}^{(n)}(t)$ and the scalar quantities $\mathbf{\Phi}^{(n)}(t) = (\phi_1^{(n)}(t),\ldots,\phi_\alpha^{(n)}(t),\ldots,\phi_{N_S}^{(n)}(t))$. Here, n is used to identify the particle, and $n = 1\ldots N_\mathrm{P}$, where N_P is the number of particles. Under Eq. (5), the Lagrangian particles evolve in the physical $(\mathbf{x})$ and scalar composition

($\mathbf{\Phi}$) spaces according to the following equations:

$$\frac{d\mathbf{x}^{(n)}}{dt} = \mathbf{U}(\mathbf{x}^{(n)}, t), \tag{6}$$

$$\frac{d\phi_\alpha^{(n)}}{dt} = \left[D_\alpha \frac{\partial^2 \phi_\alpha}{\partial x_j \partial x_j} \right]^{(n)} + S_\alpha(\mathbf{\Phi}^{(n)}), \tag{7}$$

where the first term on the right-hand side of Eq. (7) represents the effects of molecular diffusion on $\phi_\alpha^{(n)}$, and cannot be explicitly expressed by $\mathbf{\Phi}^{(n)}$ because this term contains the Laplacian operator. The second term is the reaction source term for $\phi_\alpha^{(n)}$, and is calculated from $\mathbf{\Phi}^{(n)}$ because S_α is a function of $\mathbf{\Phi}$. In the LES–LPS with the ADM, these equations are modeled using the unfiltered (resolved) velocity and the mixing model:

$$\frac{d\mathbf{x}^{(n)}}{dt} = \tilde{\mathbf{U}}(\mathbf{x}^{(n)}, t), \tag{8}$$

$$\frac{d\phi_\alpha^{(n)}}{dt} = \left[\frac{d\phi_\alpha^{(n)}}{dt} \right]_{\text{mix}} + S_\alpha(\mathbf{\Phi}^{(n)}). \tag{9}$$

The first term in Eq. (9) represents the effects of molecular diffusion modeled by the mixing model, and $[*]_{\text{mix}}$ represents that the quantity is related to the mixing model. Unlike the exact equations for $\mathbf{x}^{(n)}$ and $\mathbf{\Phi}^{(n)}$, the modeled equations do not contain the unresolved velocity in the evolution of $\mathbf{x}^{(n)}$. The LES with the ADM also assumes that the unresolved velocity in the convective term in Eq. (3) is negligible while the scalar dissipation in the unresolved scale is treated in the secondary filter. Similarly, the mixing model includes the scalar dissipation due to molecular diffusion in the scalars fields represented by the particles. The effect of the unresolved velocity was tested in planar jets by the LES–LPS with different grid sizes,[16] where the grid size was found to have only a small influence on the LPS when the large scales are resolved in the LES. We developed the mixing volume model for the molecular diffusion,[16] whose detail is described in the next subsection. It was shown that the mixing volume model in the LPS causes the SGS scalar variance to decay similarly to the secondary filter in the LES with the ADM.[16] In practice, the number of particles is limited due to the computational costs, and the simulations are often performed under the "sparse" condition[17] which means that the number of particles is much smaller than the computational grid points in the LES. The characteristics length scale of particle distributions in physical space is related to the mean distance between the nearest two particles, and is larger than the unresolved scale under the sparse condition. Therefore, the unresolved turbulent motions neglected in Eq. (8) hardly change the overall profile of the particles because the particles'

locations relative to each other are dominated by the eddies with the size comparable to the distance between the particles as confirmed in the Richardson's relative diffusion problem.[22] This is valid except for the viscous-dominant scale, which is usually in the unresolved scale in the LES. Thus, the unresolved scale is not expected to have a large influence on the particles locations relative to each other, which are important in the LPS based on the mixing model. These discussions indicate that Eq. (8) neglecting the unresolved velocity is useful in the LPS under the sparse conditions.

Mixing volume model based on two-particles interaction

The effects of molecular diffusion are modeled by the mixing volume model proposed in Watanabe et al.[16] Similarly to the conventional mixing models used in the PDF methods, the mixing volume model relies on the interaction among Lagrangian particles. However, the underlying concept is different between the mixing volume model and the conventional mixing model. The mixing volume model is formulated for spatially-distributed particles while the spatial distribution is treated as a source of the error in the conventional model.[17] Therefore, the mixing volume model is expected to show better performances even under the sparse condition, in which the distance among the mixing particles is not small. Although the original formulation of the mixing volume model is based on the interaction of spatially-distributed multiple particles, we only use the two-particles interaction model, which is practically important because of its low computational costs.[16] In the mixing volume model using two particles, the nearest particle is selected as a mixing partner. In the LPS, the mixing partner is determined for N_{P} particles. Then, the mixing scheme presented below is applied for N_{P} pairs. In this model, one particle can participate more than one mixing event per one time step. We present the IEM (Interaction by Exchange with the Mean), Curl's, and modified Curl's mixing schemes[3] for the mixing volume model. These mixing schemes themselves have been used as the mixing model. In the conventional mixing model, the separation between the mixing particles causes the numerical diffusion, which affects the decay of scalar fluctuations because of the change in the effective diffusivity coefficient.[17] In contrast, the mixing volume model yields a correct decay rate of scalar variances even if the mixing particles are spatially distributed.[16] The effects of the separation between two particles are taken into account in the mixing timescale. In the LES–LPS using the mixing

volume model based on the two-particles interaction, for $D_\alpha \approx D$, the mixing timescale τ_M for the mixing pair of the particles n and m is given by

$$\tau_\mathrm{M} = \frac{\langle \psi''^2 \rangle_{(n,m)}}{\langle N \rangle_{(n,m)}}, \tag{10}$$

where $\langle * \rangle_{(n,m)}$ denotes an average of two particles n and m (e.g., $\langle \psi \rangle_{(n,m)} = (\psi^{(n)} + \psi^{(n)})/2$), $\psi''^{(n)} = \psi^{(n)} - \langle \psi \rangle_{(n,m)}$ is the difference from average, and $N = D(\partial\psi/\partial x_j)^2$ is the scalar dissipation rate of ψ. $\langle \psi''^2 \rangle_{(n,m)}$ is estimated as $\langle \tilde{\psi}''^2 \rangle_{(n,m)}$ using the unfiltered scalar $\tilde{\psi}$ obtained by the ADM. The scalar dissipation rate N cannot be directly calculated from the resolved scalar because the contributions to N are significant in the unresolved scale. Therefore, we estimate N in Eq. (10) as $N = C_N D(\partial\overline{\psi}/\partial x_j)^2$, where C_N is a model parameter and N computed on the LES grid is interpolated to the location of the particles. This model is based on the subgrid-scale model for the scalar dissipation rate proposed by Cook and Bushe,[23] where the model parameter is dynamically determined by assuming the form of scalar energy spectrum. They showed that $C_N = O(10^0)$ by using the DNS of temporally evolving mixing layers. Unlike their model, we treat C_N as an adjustable parameter. Although C_N can be a function of space and time, a constant value of C_N is used in this study and we will show that the LES–LPS with constant C_N reproduces well the statistics measured in the experiments. C_N is determined so that the nonreactive scalar variance profiles in the LPS are consistent with those in the LES. For determining C_N, the LES–LPS is repeated by changing C_N in the range of $10^{-1} < C_N < 10^1$. Note that this method does not require any additional DNS or experiments.

When the particle n is mixed with m, the IEM mixing scheme computes the molecular diffusion term by

$$\left[d\phi_\alpha^{(n)}/dt\right]_\mathrm{mix} = \frac{1}{\tau_\mathrm{M}} \left(\langle \phi_\alpha \rangle_{(n,m)} - \phi_\alpha^{(n)} \right), \tag{11}$$

$$\left[d\phi_\alpha^{(m)}/dt\right]_\mathrm{mix} = \frac{1}{\tau_\mathrm{M}} \left(\langle \phi_\alpha \rangle_{(n,m)} - \phi_\alpha^{(m)} \right). \tag{12}$$

When dt/τ_M is larger than 1, $\phi_\alpha^{(n)}$ and $\phi_\alpha^{(m)}$ are replaced by $\langle \phi_\alpha \rangle_{(n,m)}$ instead of using Eqs. (11) and (12), where dt is the time increment. The IEM mixing scheme using two particles is related to the Curl's and modified Curl's mixing schemes by the same mixing timescale. In the Curl's mixing scheme,[24] the molecular diffusion term is modeled by following equations:

$$\left[d\phi_\alpha^{(n)}\right]_\mathrm{mix} = \beta \left[\langle \phi_\alpha \rangle_{(n,m)} - \phi_\alpha^{(n)} \right], \tag{13}$$

$$\left[d\phi_\alpha^{(m)}\right]_\mathrm{mix} = \beta \left[\langle \phi_\alpha \rangle_{(m,n)} - \phi_\alpha^{(m)} \right]. \tag{14}$$

Here, $[d\phi_\alpha^{(n)}]_{\rm mix}$ is the change in $\phi_\alpha^{(n)}$ during the time interval dt due to the molecular diffusion, and $\beta = 1$ with probability $p_{\rm mix}$ and $\beta = 0$ with probability $(1-p_{\rm mix})$. The mixing probability $p_{\rm mix}$ is given by $p_{\rm mix} = 2dt/\tau_{\rm M}$.[25] When the mixing occurs between the particles n and m, Eqs. (13) and (14) are calculated for all scalars in $\mathbf{\Phi}$, and the scalar values of the particles n and m are replaced by the averaged values $\langle\phi_\alpha\rangle_{(n,m)}$. The modified Curl's mixing scheme also uses Eqs. (13) and (14) while β and $p_{\rm mix}$ are different from the Curl's mixing scheme. In the modified Curl's mixing scheme, β is the random number between 0 and 1 which has a flat probability density function $p(\beta) = 1$.[26] The mixing probability in the modified scheme is $p_{\rm mix} = 3dt/\tau_{\rm M}$. Although the scalar variance decays according to the mixing timescale in these schemes, the simulated reactive scalars can depend on the mixing schemes.[27]

LES–LPS OF TURBULENT REACTIVE FLOWS AT HIGH SCHMIDT NUMBER

Turbulent scalar mixing layer with a chemical reaction at high Schmidt number

The LES–LPS is applied to liquid turbulent scalar mixing layers with a second-order chemical reaction $\mathrm{A} + \mathrm{B} \rightarrow \mathrm{P}$ in Fig. 1, which were experimentally investigated by Komori et al.[18,19] The turbulence is generated by a grid which consists of square bars with a thickness of 0.002 m. The mesh size M is 0.02 m. The reactants A and B are initially separated by a splitter plate in the upstream of the turbulence-generating grid, and supplied with the constant velocity $U_0 = 0.25$ m/s. The scalar mixing layer of A and B is developed behind the grid. The mixture fraction, which is independent of the reactions, can be defined as $\xi = (\Gamma_{\rm A} - \Gamma_{\rm B} + \Gamma_{\rm B0})/(\Gamma_{\rm A0} + \Gamma_{\rm B0})$, where Γ_α is the instantaneous concentration of α and $\Gamma_{\rm A0}$ and $\Gamma_{\rm B0}$ are the initial concentrations of A and B, respectively. The stoichiometric value of the mixture fraction is $\xi_{\rm S} = \Gamma_{\rm B0}/(\Gamma_{\rm A0} + \Gamma_{\rm B0})$, and the maximum concentration of P at $\xi = \xi_{\rm S}$ is $\Gamma_{\rm P0} = \Gamma_{\rm A0}\Gamma_{\rm B0}/(\Gamma_{\rm A0} + \Gamma_{\rm B0})$. The chemical source term for α, S_α, is represented by

$$S_{\rm P} = -S_{\rm A} = -S_{\rm B} = k\Gamma_{\rm A}\Gamma_{\rm B}, \tag{15}$$

where k is the chemical reaction rate constant. The source term for P normalized by $\Gamma_{\rm P0}$, M, and U_0 is $\hat{S}_{\rm P} = Da\hat{\Gamma}_{\rm A}\hat{\Gamma}_{\rm B}$, where $Da = k(\Gamma_{\rm A0} + \Gamma_{\rm B0})M/U_0$ is the Damköhler number. The experiments were conducted for three different sets of A and B. The experimental conditions are summarized in Tab. I. The case R0 is the nonreactive flow,[18,19] where the solution of

the sodium fluorescein dye ($C_{20}H_{10}Na_2O_5$) was used as species A while no chemical species are added as B. The case R1 uses the saponification reaction[18] between sodium hydroxide (NaOH: A) and methyl formate ($HCOOCH_3$: B). The case R2 uses the neutralization reaction[18,19] between acetic acid (CH_3COOH: A) and ammonium hydroxide (NH_4OH: B). Both reactions are irreversible and second-order chemical reactions without significant heat release, and the reaction rate is represented by Eq. (15) with the constant k. For the initial concentrations of R1 and R2, ξ_S is 0.5 while the Damköhler number is different. According to Komori et al.,[19] we refer R1 and R2 to as the moderately fast reaction and the rapid reaction, respectively. The experiments were conducted at the Reynolds number $Re = U_0 M/\nu$ is 5,000, and the Schmidt numbers of the diffusive species are $Sc \approx 600$. The Kolmogorov scale varies from $\eta_K/M = 1.0 \times 10^{-2}$ to 1.8×10^{-2} depending on the streamwise location, and the Batchelor scale does from $\eta_B/M = 4.1 \times 10^{-4}$ to 7.1×10^{-4}.[18,28] The dissipation spectrum for the concentration of nonreactive species[18] exhibits a peak at the length of $4.8 \times 10^{-2} M$.

Numerical methods

The schematic of the computational domain is shown in Fig. 1(b). The origin of the coordinate system is located at the center of the turbulence-generating grid. The streamwise direction and the direction vertical to the scalar mixing layer are denoted by x and y, respectively, while the z direction is parallel to the splitter plate. The grid is installed $L_{x0} = 4M$ downstream of the inflow boundary. The size of the computational domain downstream the grid is $(L_x, L_y, L_z) = (20.5M, 4M, 4M)$. According to Suzuki et al.,[29] the grid is modeled by the immersed boundary method, and the additional force term is introduced in Eq. (2) so that nonslip boundary conditions are satisfied at the grid surface. In the LES, the filtered velocity and nonreactive scalar are computed using the ADM. We consider ψ satisfying that $\psi = 1$ for $y < 0$ and $\psi = 0$ for $y > 0$ in the upstream of the grid. The boundary conditions for ψ are the same as for the mixture fraction. The diffusivity coefficients of ψ and Γ_α satisfy $Sc = 600$. The velocity fields are assumed to be periodic in the y and z directions while for the scalar fields, the periodic boundary condition is applied only in the z direction. The inflow streamwise velocity is kept constant $U = U_0$ while the velocity components parallel to the inflow plane are 0. The convective boundary condition is used at the outflow boundary ($x = L_x$). The splitter plate is assumed not to affect the

velocity fields in the simulations. Therefore, the scalar value is kept constant in the upstream of the grid without changing the velocity fields.

The present LES code is developed from the DNS code based on a finite difference method used in previous studies.[29–31] The fully conservative fourth-order central difference scheme[32] is used for spatial discretization in the y and z directions, and the fully conservative second-order central difference scheme[32] is used in the x direction. These conservative schemes reduce the dissipation caused by the numerical schemes. Equations (1) and (2) are solved using the fractional step method. The Poisson equation is solved by using the diagonal matrix algorithm along the x direction and the fast Fourier transform along the periodic (y and z) directions. The third-order Runge–Kutta method is used for the time integration. $N_x \times N_y \times N_z = 640 \times 128 \times 128$ computational grid points are used in the LES. The grid size in the x direction is reduced near the turbulence-generating grid as in DNS of grid-turbulence.[29] The computational grid sizes are $\Delta x/M = 3.7 \times 10^{-2}$ and $\Delta y/M = \Delta z/M = 3.1 \times 10^{-2}$, and are comparable to Kolmogorov scale but much larger than the Batchelor scale. This grid size is slightly smaller than in the LES of the same flow by Kurose et al.[36] The computational time step is $dt = 0.02M/U_0$. The explicit filter with a five-point stencil proposed by Stolz et al.[13] is used as the low-pass filter G. We set $N_{\mathrm{D}} = 5$ to obtain Q_N. The secondary filter $(Q_N * G)$, which removes the small-scale fluctuations, is applied to the velocity and passive scalar every N_f time steps. We set $N_f = 10$, 15, or 18 to confirm that the small-scale fluctuations are removed well by the secondary filter.

The LPS is implemented with the LES using the same procedure as in our previous study.[16] The variables computed in the LES are spatially interpolated at the particle positions by using a tri-linear interpolation. Equation (9) is solved by using the fractional step method.[16] Molecular diffusion is modeled by the mixing volume model based on two-particles interaction. The LES–LPS is performed with the IEM, Curl's, or modified Curl's mixing scheme. For R1, $\mathbf{\Phi} = (\xi, \Gamma_{\mathrm{P}})$ are computed in the LPS while the concentrations of A and B are obtained from the conservation laws as $\Gamma_{\mathrm{A}} = \Gamma_{\mathrm{A0}}\xi - \Gamma_{\mathrm{P}}$ and $\Gamma_{\mathrm{B}} = \Gamma_{\mathrm{B0}}(1-\xi) - \Gamma_{\mathrm{P}}$.[33] The Damköhler number in R2 is very large, which requires a very small computational time step because of the small reaction timescale. Therefore, we compute the concentrations of reactive species from the mixture fraction using the equilibrium limit ($Da \to \infty$) in the

conserved scalar theory[33,34] as follows.

$$\lim_{Da\to\infty} \Gamma_{\rm A} = (\Gamma_{\rm A0} + \Gamma_{\rm B0})(\xi - \xi_{\rm S})H(\xi - \xi_{\rm S}), \tag{16}$$

$$\lim_{Da\to\infty} \Gamma_{\rm B} = (\Gamma_{\rm A0} + \Gamma_{\rm B0})(\xi_{\rm S} - \xi)H(\xi_{\rm S} - \xi), \tag{17}$$

$$\lim_{Da\to\infty} \Gamma_{\rm P} = \begin{cases} \Gamma_{\rm A0}\xi & (\xi < \xi_{\rm S}) \\ \Gamma_{\rm B0}(1-\xi) & (\xi \geq \xi_{\rm S}) \end{cases}. \tag{18}$$

Here, $H(z)$ is the step function which satisfies $H(z) = 1$ for $z \geq 0$ and $H(z) = 0$ for $z < 0$.

Initially, the particles are randomly placed in the computational domain except the inside the turbulence-generating grid. In the upstream of the grid, the particles with $y^{(n)} < 0$ are forced to be $\Gamma_{\rm A}^{(n)} = \Gamma_{\rm A0}$ and $\Gamma_{\rm B}^{(n)} = \Gamma_{\rm P}^{(n)} = 0$ while those with $y^{(n)} > 0$ are forced to be $\Gamma_{\rm B}^{(n)} = \Gamma_{\rm B0}$ and $\Gamma_{\rm A}^{(n)} = \Gamma_{\rm P}^{(n)} = 0$. In the downstream of the grid ($x > 0$), the scalars evolve according to their transport equations. A periodic boundary condition is applied to the position of particles in the y and z direction. Once a particle crosses the boundary at $z = L_z/2$ ($-L_z/2$), it enters into the computational domain through $z = -L_z/2$ ($z = L_z/2$) without changing the scalar values $\Gamma_\alpha^{(n)}$. For a particle crossing the boundary at $y = L_y/2$, the particle enters the computational domain from the boundary at $y = -L_y/2$ with $\Gamma_{\rm A}^{(n)} = \Gamma_{\rm A0}$ and $\Gamma_{\rm B}^{(n)} = \Gamma_{\rm P}^{(n)} = 0$. Similarly, the particle enters the computational domain from the boundary at $y = L_y/2$ with $\Gamma_{\rm B}^{(n)} = \Gamma_{\rm B0}$ and $\Gamma_{\rm A}^{(n)} = \Gamma_{\rm P}^{(n)} = 0$. For the particles, the y–z plane at $x = -L_{x0}$ is the inflow boundary, whereas the y–z plane at $x = L_x$ is the outflow boundary. A particle that leaves the computational domain across the inflow or outflow boundary is replaced on the inflow boundary. Because the velocity on the inflow boundary is constant ($U = U_0$), the particle is randomly replaced on the inflow boundary.

The number of particles $N_{\rm P}$ determines the spatial resolution of the LPS. The LPS is performed for $N_{\rm P} = 40,000$, $80,000$, and $120,000$ with the modified Curl's model. The LPS with $N_{\rm P} = 80,000$ is used for investigating the dependence of LES–LPS on C_N and the mixing schemes. Table II summarizes the numerical parameters relating to $N_{\rm P}$: the number density of particles, $\rho_{\rm P} = N_{\rm P}/[(L_{x0} + L_x) \times L_y \times L_z]$, the mean distance between the nearest particles, $\delta_{\rm P} = (4\pi\rho_{\rm P}/3)^{-1/3}$, and the grid number in the LES occupied by one particle, $(N_x \times N_y \times N_z)/N_{\rm P}$. $N_{\rm P}$ is smaller than the number of the computational grid points in the LES, and the LES–LPS is performed under the sparse condition.

In the LES, the velocity statistics are calculated by taking time average and average on y–z planes as a function of x while the scalar statistics are calculated by taking time average

and z direction average as a function of (x, y). In the LPS, the computational domain is divided into 130×100 grid cells in the x and y directions. Then, statistics are calculated in each cell by taking the cloud-in-cell ensemble average[3] (i.e., the ensemble average of particles located in the cell).

We summarize the simulated quantities here. The velocity and nonreactive scalar in the LES are denoted U_i and ψ, respectively. The mixture fraction ξ, which is also independent of the reactions, and the concentrations Γ_α are simulated in the LPS. The same boundary conditions are applied for ψ and ξ.

RESULTS AND DISCUSSION

LES results

Before we discuss the statistics of the reactive scalars in the LPS, we compare the statistics of velocity and nonreactive scalar between the experiments and the LES with ADM. In the LES, the average value $\langle f \rangle$ is estimated from the unfiltered value as $\langle \tilde{f} \rangle = \langle Q_N * \overline{f} \rangle$ to take the subfilter scale into account. Figure 2 shows the streamwise decay of turbulent intensity $\langle {u_i}^2 \rangle$, where $u_i = U_i - \langle U_i \rangle$ is the fluctuating component of velocity. The turbulent intensity is compared among the LES with $N_f = 10$, 15, and 18. The LES results agree with the experiments, and hardly depend on N_f. The independence of N_f shows that the explicit filter removes the energy well from the small scale on the computational grid without affecting the large-scale fields, which have large contributions to the turbulent intensity. These results show that the LES with the ADM can be a useful tool to simulate turbulent flows generated by grid objects.

Figure 3 compares the nonreactive scalar statistics between the experiments and the LES, where $\psi' = \psi - \langle \psi \rangle$ is the scalar fluctuation. The mixture fraction statistics in the experiments are used here. As shown in Figs. 3(a) and (b), the LES well predicts the mean development of scalar mixing layer and the streamwise evolution of the rms scalar fluctuation. The vertical turbulent scalar flux in the LES also agrees well with the experiment (Fig. 3(c)). The large-scale energy-containing eddies dominate the turbulent scalar flux.[35] Thus, the present LES resolves the large-scale motions which are important in the evolution of the Lagrangian particles.

Nonreactive scalar statistics in LPS

Because the LPS is performed combined with the LES, the nonreactive scalar variance in the LPS, $\langle \xi'^2 \rangle$, should be consistent with the one in the LES, $\langle \psi'^2 \rangle$. An adequate value of the parameter C_N is determined from $\langle \xi'^2 \rangle$ and $\langle \psi'^2 \rangle$. Figure 4(a) shows the dependence of $\langle \xi'^2 \rangle^{1/2}$ on C_N with $\langle \psi'^2 \rangle^{1/2}$ in the LES at $(x, y) = (12M, 0)$. The scalar variance in the LPS decreases with C_N. $\langle \xi'^2 \rangle^{1/2}$ is close to the LES value for $C_N \sim 10^0$, and therefore we use $C_N = 1.6$ hereafter. This value is quite similar to the DNS results of mixing layers,[23] where $C_N = 1.3$–2.0. Note that because $\langle \xi'^2 \rangle^{1/2}$ slowly changes with C_N, a slightly different value of C_N provides a similar results to the LES–LPS with $C_N = 1.6$.

Figure 4(b) shows the dependence of the scalar variance on the mixing schemes. The mixing volume model was developed so that it yields the same decay rate of scalar variance for any mixing schemes independently of the number of particles. Indeed, we can find in Fig. 4(b) that $\langle \xi'^2 \rangle$ is independent of the choice of the mixing schemes. The effects of the two-particles mixing scheme depend on the distance between the mixing particles d_M.[17] Therefore, the mixing timescale τ_M should be an implicit function of d_M to take into account the d_M dependence of the mixing schemes. Because the nearest particle is chosen as the mixing partner, $\langle d_\mathrm{M} \rangle = \delta_\mathrm{P}$ changes with the number of particles used in the LPS as shown in Tab. II. Figure 4(c) compares $\langle \xi'^2 \rangle$ among the LPS with $N_\mathrm{P} = 40,000$, $80,000$, and $120,000$, where the modified Curl's scheme is used in all simulations. Figure 4(d) shows the mean mixing timescale $\langle \tau_\mathrm{M} \rangle$ on the centerline. The scalar variance in the LPS is almost independent of N_P. Similar to the LES–LPS of planar jets at $Sc = 1$, $\langle \tau_\mathrm{M} \rangle$ decreases as N_P increases (as δ_P becomes small). Figures 4(b) and (c) compare the nonreactive scalar variances between the LES and the LPS. Both simulations show almost the same profiles, indicating that the mixing volume model is capable to model the molecular diffusion at high Schmidt numbers under various numerical conditions. Thus, even at high Sc, the mixing volume model yields a correct decay rate of scalar variance for different δ_P by adjusting τ_M.

Reactive scalar statistics in LPS

Figure 5 shows the mean concentrations of A and P on the centerline in the LES–LPS with the modified Curl's scheme for $N_\mathrm{P} = 40,000$ and $120,000$. The LES–LPS results are

independent of N_{P} and agree well with the experiments for both moderately fast reaction R1 and rapid reaction R2. The present liquid scalar mixing layers experimentally investigated by Komori et al.[18,19] have been used to validate the numerical methods for reactive flows. Kurose et al.[36] applied the LES with flamelet approaches while Michioka et al.[2] applied the LES with the SGS models for the filtered reaction source terms. Their LES simulated both velocity and reactive scalars using the computational grid in the Eulerian frame. Because of the lack of the spatial resolutions near the turbulence-generating grid, where a large scalar gradient appears behind the splitter plate, their LES overpredicts the mean concentration of P near the grid. Unlike their grid-based LES of reactive scalars, $\langle \Gamma_\alpha \rangle$ in the LPS near the grid smoothly connects to the experimental plots in the downstream region, and the LPS can predict well the reaction in the region with a large scalar gradient even under the sparse condition.

Figure 6(a) shows $\langle \Gamma_{\mathrm{P}} \rangle$ on the centerline obtained from the LES–LPS with $C_N = 1.2$, 1.6, and 2.0. It is found that the dependence of $\langle \Gamma_{\mathrm{P}} \rangle$ on C_N is not significant for $C_N \approx 1.6$. Figure 6(b) compares $\langle \Gamma_{\mathrm{P}} \rangle$ among the LES–LPS using different mixing schemes. While $\langle \Gamma_{\mathrm{P}} \rangle$ for R1 hardly changes with the mixing schemes, the LES–LPS with the Curl's mixing scheme overpredicts $\langle \Gamma_{\mathrm{P}} \rangle$ for R2 compared with the other schemes. The reaction rate for the rapid reaction, R2, is controlled by the mixing process. Therefore, for the rapid reaction, the mixing scheme has great influences on the reactive scalar statistics in the LPS although the decay rate of nonreactive scalar variance is almost the same for all mixing schemes.

For the second-order reaction, the characteristics of mixing and reaction are often investigated by the correlation of concentration fluctuations $\langle \gamma_{\mathrm{A}} \gamma_{\mathrm{B}} \rangle$, where $\gamma_\alpha = \Gamma_\alpha - \langle \Gamma_\alpha \rangle$ is the concentration fluctuation. In the RANS approach for turbulent reactive flows, the models are used for the concentration correlation to close the averaged scalar transport equations.[33] Komori et al.[19] also measured the concentration correlation coefficient $C_{\mathrm{AB}} = \langle \gamma_{\mathrm{A}} \gamma_{\mathrm{B}} \rangle / \sqrt{\langle \gamma_{\mathrm{A}}^2 \rangle \langle \gamma_{\mathrm{B}}^2 \rangle}$ and the segregation intensity $I_{\mathrm{S}} = \langle \gamma_{\mathrm{A}} \gamma_{\mathrm{B}} \rangle / \langle \Gamma_{\mathrm{A}} \rangle \langle \Gamma_{\mathrm{B}} \rangle$ in the reactive scalar mixing layers. From the definitions, C_{AB} and I_{S} have a value between -1 and 0. In nonreactive flows, $C_{\mathrm{AB}} = -1$ because $\gamma_{\mathrm{A}} = -\gamma_{\mathrm{B}}$, and the reactions cause C_{AB} to increase. Figure 7(a) compares C_{AB} among the experiment and the LES–LPS with three mixing schemes. For R1, the LES–LPS shows good agreement with the experiment for all mixing schemes. While the Curl's mixing scheme overpredicts the effects of the reaction on C_{AB} for R2, the LES–LPS with the IEM and modified Curl's mixing schemes predicts better C_{AB} for

R2. Figure 7(b) shows I_S on the centerline. $I_S = -1$ when the two reactants do not coexist while $I_S = 0$ when they are completely and ideally mixed. Thus, I_S can be considered as a measure of the unmixedness of the two reactants. For the infinitely fast reaction, such as R2 in the present flow, the concentration of one of the two reactants is always 0, resulting in $I_S = -1$. Previous studies on reactive flows with a second-order reaction revealed that the chemical reaction reduces I_S because the presence of the chemical product causes the two reactants to be segregated.[19,33,37] As shown in Fig. 7(b), I_S for R0 increases in the downstream direction because of the progress of the mixing, while the reaction makes I_S small. The LES–LPS shows good agreement with the experiment for all Da considered in this study. Thus, the LES–LPS is capable to predict the mixing states of the reactants in the turbulent flows where the mixing and reaction simultaneously proceed.

We compare the vertical profiles of concentration statistics between the experiment[18] and the LES–LPS with $N_P = 80,000$ and the modified Curl's scheme. In the experiment by Komori et al.[18] the vertical profiles are measured only for R0 and R2. Figure 8 shows the vertical profiles of $\langle \Gamma_A \rangle$. The vertical coordinate y is normalized by the mixing layer thickness δ for investigating the inside of the mixing layer, where the reaction takes place. The thickness δ is estimated from the mean mixture fraction profile $\langle \xi \rangle$ as the distance between the vertical locations of $\langle \xi \rangle = 0.1$ and 0.9. The difference between the reactive and nonreactive cases increases in the streamwise direction, and the changes due to the reaction are predicted well in the LES–LPS. Figure 9 compares the variance of concentration $\langle \gamma_A^2 \rangle$ and the vertical turbulent flux $\langle v\gamma_A \rangle$ for the reactant A at $x/M = 20$. In the lower side of the mixing layer ($y < 0$), both $\langle \gamma_A^2 \rangle$ and $\langle v\gamma_A \rangle$ are increased owing to the reaction while they are decreased in the upper side ($y > 0$). For the second-order reaction, in the region where the reactant is lean, the reaction tends to suppress the concentration fluctuation of the reactant and the opposite effects exist in the rich region.[34] Because the reactant A is supplied from the lower side, $\langle \gamma_A^2 \rangle$ and $\langle v\gamma_A \rangle$ are increased by the reaction in this rich side. These changes in $\langle \gamma_A^2 \rangle$ and $\langle v\gamma_A \rangle$ are well predicted by the LES–LPS. The changes in mean concentrations and turbulent scalar fluxes due to the reaction are related to the closure problem of averaged reactive scalar transport equations, where the turbulent diffusion term is often modeled using the gradient diffusion hypothesis.[38] The progress of reactions has strong influences on turbulent diffusions of reactive scalars.[39] The present results show that the LES–LPS predicts well the characteristics of turbulent diffusions of reactive scalars.

CONCLUSIONS

The LES–LPS with the ADM and mixing volume model was applied to the second-order irreversible isothermal reaction in the turbulent scalar mixing layers behind the turbulence-generating grid at high Schmidt number $Sc = 600$. The simulations were performed for the flows with no reaction, moderately fast reaction, and rapid reaction. The IEM, Curl's, and modified Curl's mixing schemes were tested for the mixing volume model based on two-particles interaction. The LES–LPS results were compared with the experiments.[18,19] The comparison showed that the velocity and nonreactive scalar statistics are well predicted in the grid turbulence by the LES with the ADM. The nonreactive scalar variance in the LPS is independent of the number of particles, which determines the length scale of the mixing event, indicating that the effects of the separation between the mixing particles are taken into account in the mixing timescale even at high Sc. Thus, the mixing volume model is capable to model the molecular diffusion at high Sc. The LES–LPS and the experiments were compared based on the statistics of reactive scalars, such as mean concentration, scalar variance, turbulent scalar flux, and concentration correlation. These statistics show good agreement for both moderately fast reaction and rapid reaction between the LES–LPS and the experiments when the IEM or modified Curl's mixing scheme is used in the mixing volume model. The LES–LPS with the Curl's mixing scheme overpredicts the effect of the rapid reaction while it predicts well the above statistics for the moderately fast reaction. The present results showed that the LES–LPS with the ADM and mixing volume model is applicable to turbulent flows with chemical reactions at high Schmidt numbers.

ACKNOWLEDGMENTS

The authors would like to thank Prof. Yasuhiko Sakai, Dr. Takashi Kubo, and Dr. Osamu Terashima for their help in this study. This work was supported by and MEXT KAKENHI Grant Number 25289030.

TABLE I. Experimental conditions in Komori et al.[18,19]

Case	Reaction rate constant	Γ_{A0}	Γ_{B0}	Γ_{P0}	ξ_S	Da
R0:	–	5.0×10^{-3} mol/m^3	0 mol/m^3	–	–	0
R1:	$k = 0.047$ m^3/(mol·s)	100 mol/m^3	100 mol/m^3	50 mol/m^3	0.5	0.751
R2:	$k = 10^8$ m^3/(mol·s)	10 mol/m^3	10 mol/m^3	5 mol/m^3	0.5	$O(10^8)$

TABLE II. Computational parameters relating to the number of particles N_P in the LES–LPS.

N_P	ρ_P	δ_P	$(N_x \times N_y \times N_z)/N_P$
40,000	$102M^{-3}$	$0.13M$	262
80,000	$204M^{-3}$	$0.11M$	131
120,000	$306M^{-3}$	$0.092M$	87

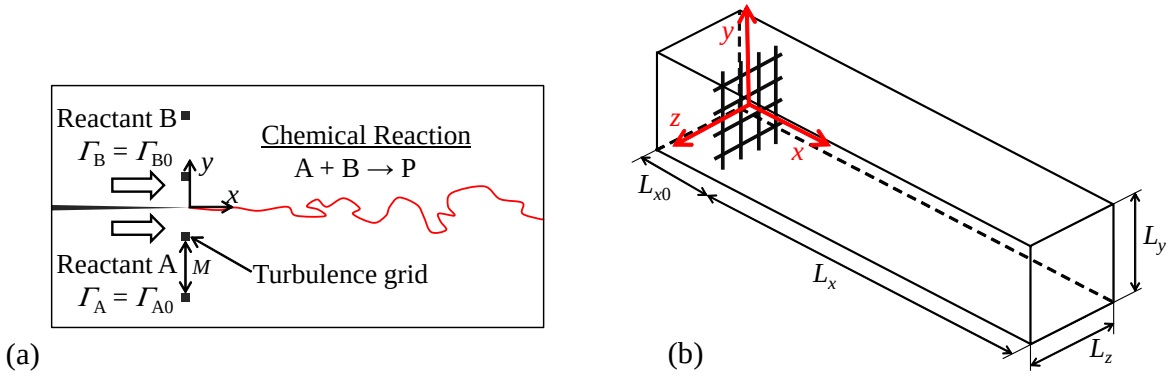

FIG. 1. (a) Turbulent reactive mixing layer behind turbulence-generating grid. The two reactants A and B are separated by the splitter plate in the upstream of the grid. (b) Schematic of computational domain.

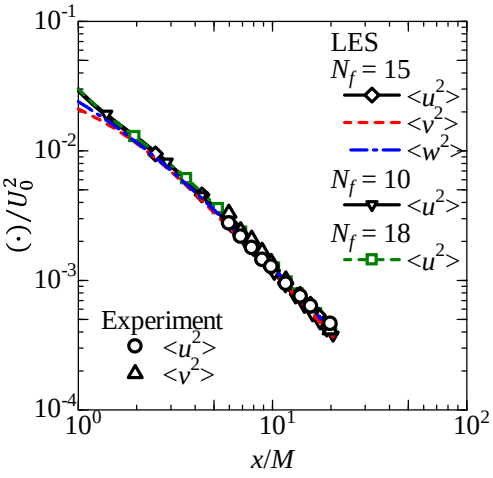

FIG. 2. Streamwise decay of turbulent intensity. The LES results with $N_f = 10$, 15, and 18 are compared with the experimental results.[18]

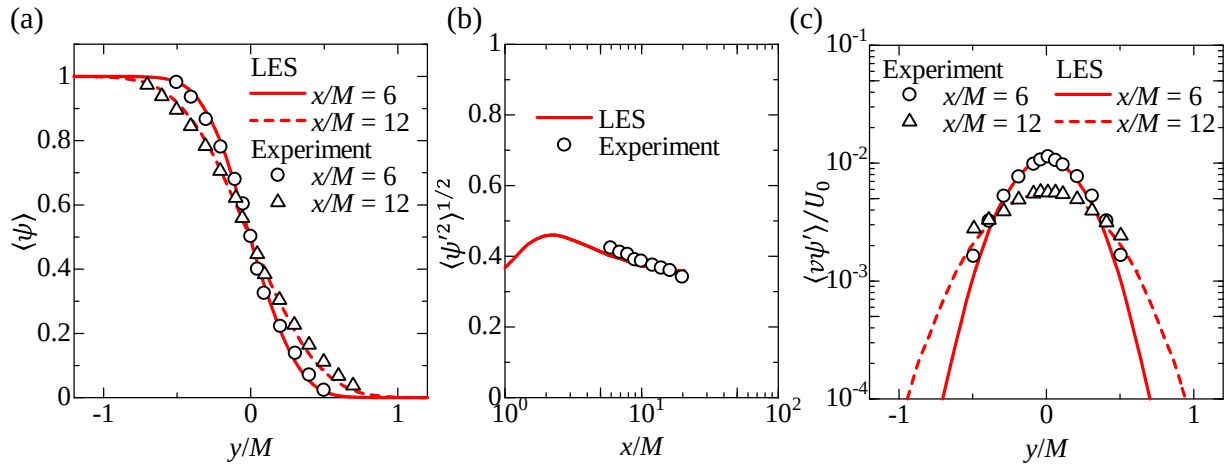

FIG. 3. Comparison of nonreactive scalar statistics between LES and experiments.[18] (a) Vertical profiles of mean scalar $\langle\psi\rangle$ at $x/M = 6$ and 12. (b) Streamwise evolution of rms scalar fluctuation $\langle\psi'^2\rangle^{1/2}$ on the centerline. (c) Vertical profiles of vertical turbulent scalar flux $\langle v\psi'\rangle$ at $x/M = 6$ and 12

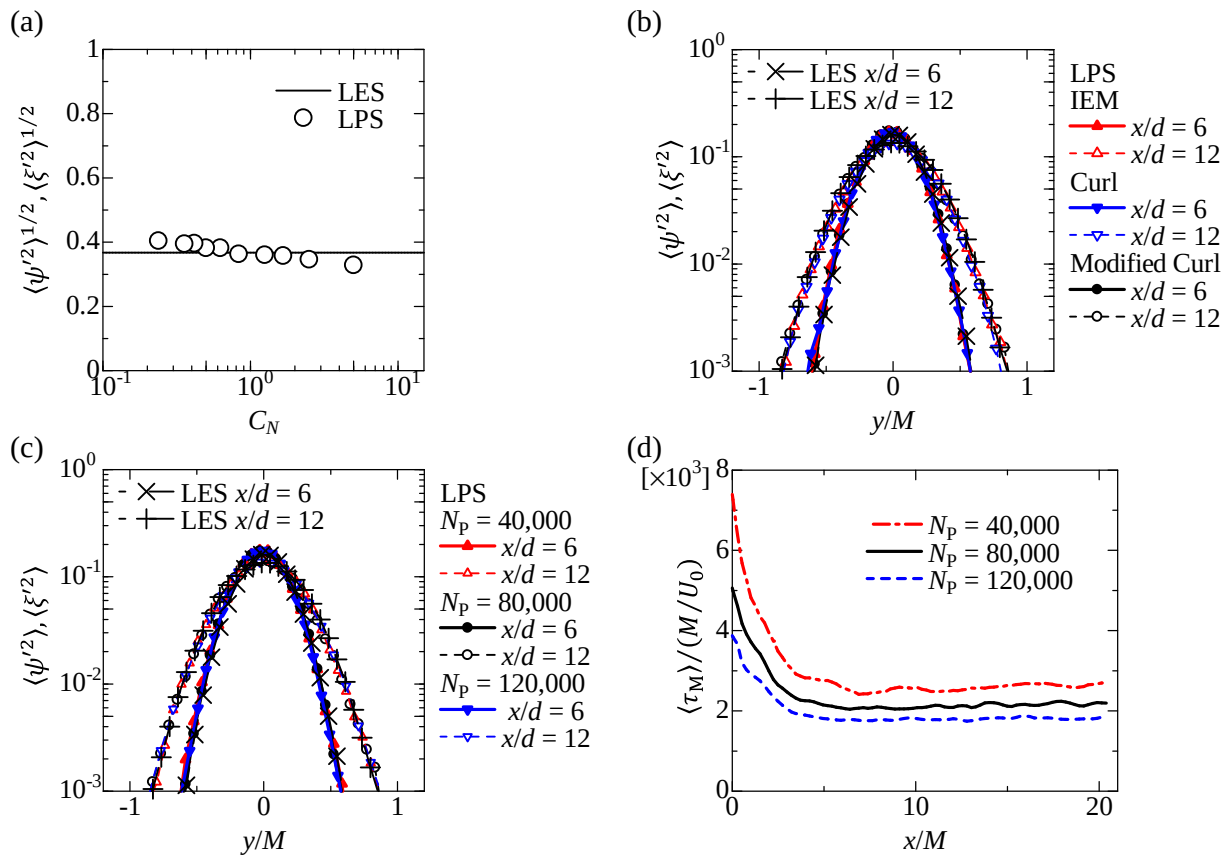

FIG. 4. (a) Rms nonreactive scalar fluctuation in LES ($\langle\psi'^2\rangle^{1/2}$) and LPS ($\langle\xi'^2\rangle^{1/2}$) at $(x, y) = (12M, 0)$ as a function of C_N. Vertical profiles of nonreactive scalar variance are compared between LES and LPS: (b) dependence on the mixing schemes ($N_\mathrm{P} = 80,000$) and (c) dependence on the number of particles N_P (the modified Curl's mixing scheme). (d) Mean mixing timescale $\langle\tau_\mathrm{M}\rangle$ on the centerline in the simulations with $N_\mathrm{P} = 40,000$, $80,000$, and $120,000$.

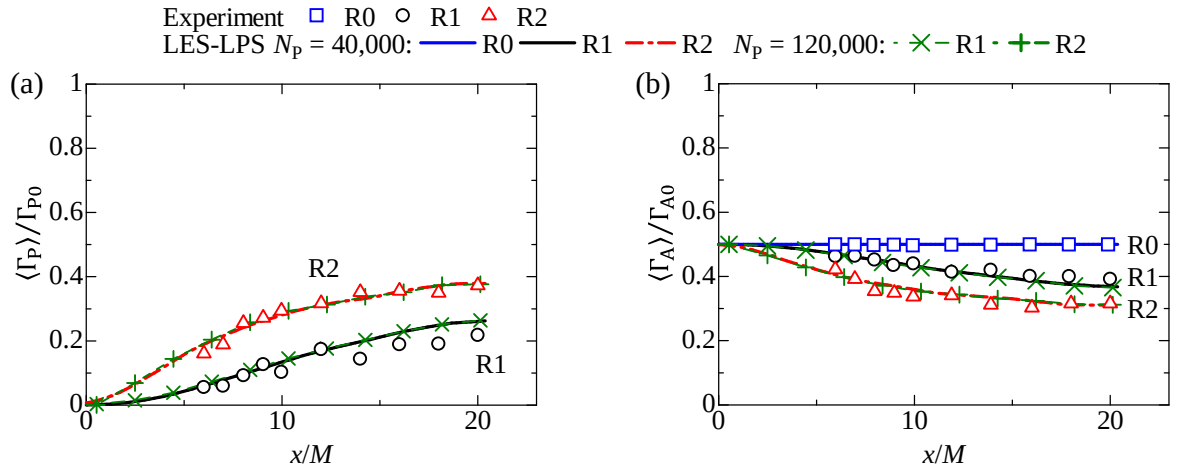

FIG. 5. Mean concentrations of (a) product P and (b) reactant A on the centerline. The dependence of the mean concentrations on the number of particles are shown for the LES–LPS with the modified Curl's mixing scheme.

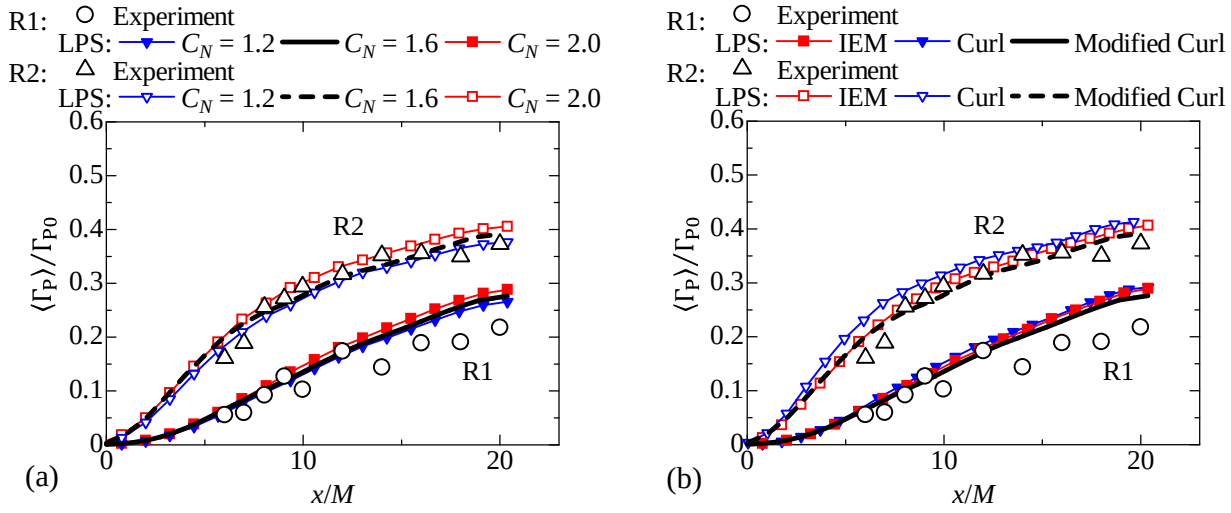

FIG. 6. Mean concentrations of product P on the centerline. (a) Dependence on C_N (the modified Curl's mixing scheme, $N_P = 80,000$). (b) Dependence on the mixing schemes ($N_P = 80,000$). The experimental results[19] are compared with the LES–LPS.

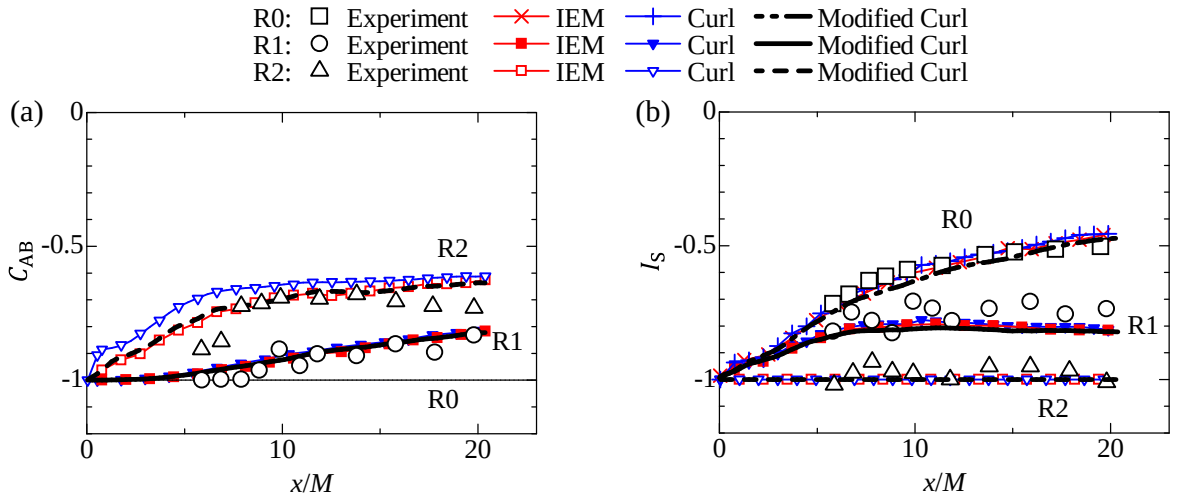

FIG. 7. Joint statistics between concentrations of A and B: (a) correlation coefficient $C_{\mathrm{AB}} = \langle \gamma_{\mathrm{A}} \gamma_{\mathrm{B}} \rangle / \sqrt{\langle \gamma_{\mathrm{A}}^2 \rangle \langle \gamma_{\mathrm{B}}^2 \rangle}$ and (b) segregation intensity $I_{\mathrm{S}} = \langle \gamma_{\mathrm{A}} \gamma_{\mathrm{B}} \rangle / \langle \Gamma_{\mathrm{A}} \rangle \langle \Gamma_{\mathrm{B}} \rangle$. The experimental results[19] are compared with the LES–LPS using the IEM, Curl's, and modified Curl's mixing schemes ($N_{\mathrm{P}} = 80,000$).

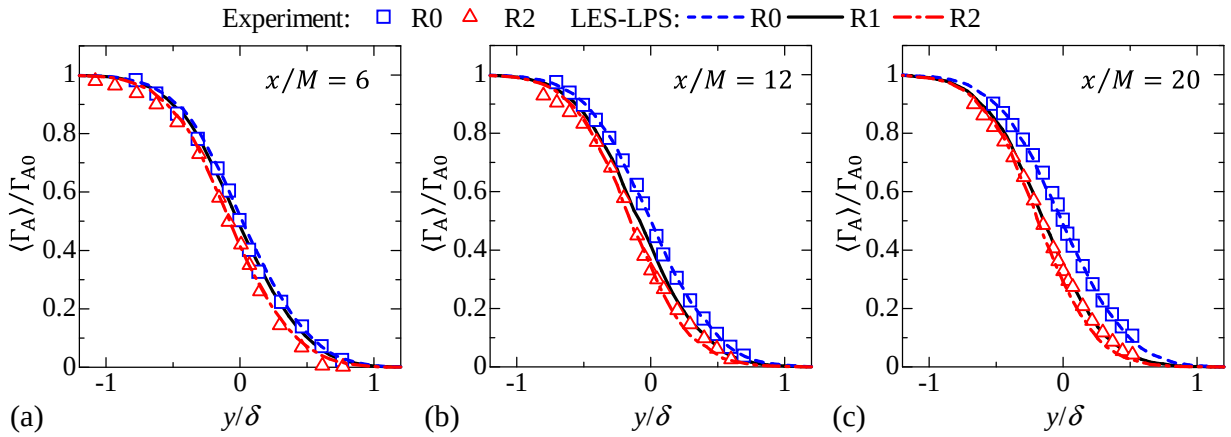

FIG. 8. Vertical profiles of mean concentration of reactant A at (a) $x/M = 6$, (b) $x/M = 12$, and (c) $x/M = 20$. The results in the LES–LPS with the modified Curl's mixing scheme and $N_P = 80,000$ particles are compared with the experiments[18] for R0 and R2.

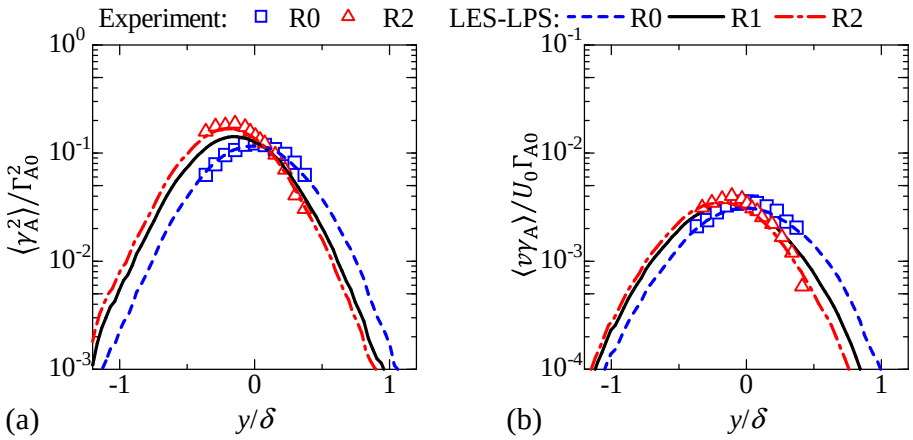

FIG. 9. Vertical profiles of (a) concentration variance $\langle\gamma_{\rm A}^2\rangle$ and (b) vertical turbulent flux $\langle v\gamma_{\rm A}'\rangle$ of concentration of reactant A at $x/M = 20$. The results in the LES–LPS with the modified Curl's mixing scheme and $N_P = 80,000$ particles are compared with the experiments[18] for R0 and R2.

REFERENCES

[1]Pitsch H. Large-eddy simulation of turbulent combustion. *Annu Rev Fluid Mech.* 2006;38:453–482.

[2]Michioka T, Komori S. Large-Eddy simulation of a turbulent reacting liquid flow. *AIChE J.* 2004;50:2705–2720.

[3]Fox RO. *Computational Models for Turbulent Reacting Flows.* Cambridge Univ. Pr. 2003.

[4]Schumann U. Large-eddy simulation of turbulent diffusion with chemical reactions in the convective boundary layer. *Atmos Environ.* 1989;23:1713–1727.

[5]Haworth DC. Progress in probability density function methods for turbulent reacting flows. *Prog Energy Combust Sci.* 2010;36:168–259.

[6]Moin P, Squires K, Cabot W, Lee S. A dynamic subgrid-scale model for compressible turbulence and scalar transport. *Phys Fluids A.* 1991;3:2746–2757.

[7]Bogey C, Bailly C. Decrease of the effective Reynolds number with eddy-viscosity subgrid modeling. *AIAA J.* 2005;43:437–439.

[8]Schlatter P, Stolz S, Kleiser L. LES of transitional flows using the approximate deconvolution model. *Int J Heat Fluid Flow.* 2004;25:549–558.

[9]Le Ribault C, Sarkar S, Stanley SA. Large eddy simulation of a plane jet. *Phys Fluids.* 1999;11:3069–3083.

[10]da Silva CB. The behavior of subgrid-scale models near the turbulent/nonturbulent interface in jets. *Phys Fluids.* 2009;21:081702.

[11]Stolz S, Adams NA. An approximate deconvolution procedure for large-eddy simulation. *Phys Fluids.* 1999;11:1699–1701.

[12]Domaradzki JA, Adams NA. Direct modelling of subgrid scales of turbulence in large eddy simulations. *J Turbulence.* 2002;3:1.

[13]Stolz S, Adams NA, Kleiser L. An approximate deconvolution model for large-eddy simulation with application to incompressible wall-bounded flows. *Phys Fluids.* 2001;13:997–1015.

[14]Ziefle J, Kleiser L. Large-eddy simulation of a round jet in crossflow. *AIAA J.* 2009;47:1158–1172.

[15]Stolz S, Adams NA. Large-eddy simulation of high-Reynolds-number supersonic boundary layers using the approximate deconvolution model and a rescaling and recycling technique.

Phys Fluids. 2003;15:2398–2412.

[16]Watanabe T, Sakai Y, Nagata K, Ito Y, Hayase T. LES–Lagrangian particle method for turbulent reactive flows based on the approximate deconvolution model and mixing model. *J Comput Phys.* 2015;294:127–148.

[17]Klimenko AY. Lagrangian particles with mixing. II. Sparse-Lagrangian methods in application for turbulent reacting flows. *Phys Fluids.* 2009;21:065102.

[18]Komori S, Nagata K, Kanzaki T, Murakami Y. Measurements of mass flux in a turbulent liquid flow with a chemical reaction. *AIChE J.* 1993;39:1611–1620.

[19]Komori S, Kanzaki T, Murakami Y. Concentration correlation in a turbulent mixing layer with chemical reactions. *J Chem Eng Jpn.* 1994;27:742–748.

[20]Mathew J, Lechner R, Foysi H, Sesterhenn J, Friedrich R. An explicit filtering method for large eddy simulation of compressible flows. *Phys Fluids.* 2003;15:2279–2289.

[21]Bogey C, Bailly C. Turbulence and energy budget in a self-preserving round jet: direct evaluation using large eddy simulation. *J. Fluid Mech.* 2009;627:129–160.

[22]Davidson PA. *Turbulence: An Introduction for Scientists and Engineers.* Oxford Univ. Pr. 2004.

[23]Cook AW, Bushe WK. A subgrid-scale model for the scalar dissipation rate in nonpremixed combustion. *Phys Fluids.* 1999;11:746.

[24]Curl RL. Dispersed phase mixing: I. Theory and effects in simple reactors. *AIChE J.* 1963;9:175–181.

[25]Correa SM. A direct comparison of pair-exchange and IEM models in premixed combustion. *Combust Flame.* 1995;103:194–206.

[26]Janicka J, Kolbe W, Kollmann W. Closure of the transport equation for the probability density funcfion of turbulent scalar fields. *J Nonequil Thermodyn.* 1979;4:47–66.

[27]Mitarai S, Riley JJ, Kosaly G. Testing of mixing models for Monte Carlo probability density function simulations. *Phys Fluids.* 2005;17:047101. mitarai2005testing

[28]Komori S, Kanzaki T, Makami Y, Ueda H. Simultaneous measurements of instantaneous concentrations of two species being mixed in a turbulent flow by using a combined laser-induced fluorescence and laser-scattering technique. *Phys Fluids.* 1989;1:349–352.

[29]Suzuki H, Nagata K, Sakai Y, Hayase T, Hasegawa Y, Ushijima T. Direct numerical simulation of fractal-generated turbulence. *Fluid Dyn Res.* 2013;45:061409.

[30]Watanabe T, Sakai Y, Nagata K, Ito Y, Hayase T. Turbulent mixing of passive scalar near turbulent and non-turbulent interface in mixing layers. *Phys Fluids.* 2015;27:085109.

[31]Watanabe T, da Silva CB, Sakai Y, Nagata K, Hayase, T. Lagrangian properties of the entrainment across turbulent/non-turbulent interface layers. *Phys Fluids.* 2016;28:031701.

[32]Morinishi Y, Lund TS, Vasilyev OV, Moin P. Fully conservative higher order finite difference schemes for incompressible flow. *J Comput Phys.* 1998;143:90–124.

[33]Watanabe T, Sakai Y, Nagata K, Terashima O. Experimental study on the reaction rate of a second-order chemical reaction in a planar liquid jet. *AIChE J.* 2014;60:3969-3988.

[34]Bilger RW, Saetran LR, Krishnamoorthy LV. Reaction in a Scalar Mixing Layer. *J Fluid Mech.* 1991;233:211–242.

[35]Komori S, Nagata K. Effects of molecular diffusivities on counter-gradient scalar and momentum transfer in strongly stable stratification. *J Fluid Mech.* 1996;326:205–237.

[36]Kurose R, Michioka T, Kohno N, Komori S, Baba Y. Application of flamelet model to large-eddy simulation of turbulent reacting liquid flows. *AIChE J.* 2011;57:911–917.

[37]Chorny AD, Zhdanov VL. Verification of chemical reaction rate models in turbulent reacting flows at Schmidt number considerably exceeding 1. *J Eng Phys Thermophys.* 2010;83:513–524.

[38]Combest DP, Ramachandran PA, Dudukovic MP. On the gradient diffusion hypothesis and passive scalar transport in turbulent flows. *Ind Eng Chem Res.* 2011;50:8817–8823.

[39]Elperin T, Kleeorin N, Liberman M, Rogachevskii I. Turbulent diffusion of chemically reacting gaseous admixtures. *Phys Rev E.* 2014;90:053001.